Available online at www.sciencedirect.com

ScienceDirect

IFAC Papers Online CONFERENCE PAPER ARCHIVE

IFAC PapersOnLine 56-2 (2023) 2871–2876

Path Planning for Concentric Tube Robots: A Toolchain with Application to Stereotactic Neurosurgery ⋆

Matthias K. Hoffmann * **Willem Esterhuizen** * ** **Karl Worthmann** ** **Kathrin Flaßkamp** *

* *Systems Modeling and Simulation, Systems Engineering, Universität des Saarlandes, Germany (e-mail: kathrin.flasskamp/matthias.hoffmann@uni-saarland.de).*

** *Optimization-based Control Group, Institute of Mathematics, Technische Universität Ilmenau, Germany (e-mail: willem-daniel.esterhuizen/karl.worthmann@tu-ilmenau.de)*

Abstract: We present a toolchain for solving path planning problems for concentric tube robots through obstacle fields. First, ellipsoidal sets representing the target area and obstacles are constructed from labelled point clouds. Then, the nonlinear and highly nonconvex optimal control problem is solved by introducing a homotopy on the obstacle positions where at one extreme of the parameter the obstacles are removed from the operating space, and at the other extreme they are located at their intended positions. We present a detailed example (with more than a thousand obstacles) from stereotactic neurosurgery with real-world data obtained from labelled MRI scans.

Keywords: optimal control, non-linear programming, homotopy methods, optimal path planning, concentric tube robots, stereotactic neurosurgery

1. INTRODUCTION

Concentric-tube continuum robots possess great potential to improve stereotactic surgery (that is, minimally-invasive procedures), due to their ability to trace out curved paths in the body. This is particularly true in neurosurgery where it may be desirable to reach a target area while avoiding various sensitive structures and blood vessels of the brain. The modelling and control of concentric tube robots have received a lot of attention, see Gilbert et al. (2016) for a review. Models of such robots range from those derived from kinematic and/or geometric arguments, such as in Dupont et al. (2009), Bergeles et al. (2015) and Granna et al. (2019), to more complicated ones involving physical effects due to bending and torsion of the tubes, as in Webster et al. (2006) and Rucker (2011). The papers Greiner-Petter and Sattel (2017) and Ha et al. (2018) aim at also describing certain nonlinear effects.

Much research has been done on path planning for concentric tube robots, with a particular focus on stereotactic surgery. Using a model from Webster et al. (2009), the paper by Lyons et al. (2009) is able to state the path planning problem as a finite dimensional optimization problem. A "sample-based motion planning" approach is presented by Torres and Alterovitz (2011) where the problem is addressed with rapidly exploring roadmaps that use the model by Rucker (2011). Also using the model from Rucker (2011), and applying a sample-based approach, the paper Burgner et al. (2013) tries to maximise the volume reachable by the tube tip subject to a constrained workspace. The paper by Peikert et al. (2022) addresses the problem by finding paths of connected voxels (a 3D pixel) that the robot can traverse, subject to constraints on its curvature. Flaßkamp et al. (2019) consider obstacle-avoiding path planning in neurosurgery for a tube robot in two dimensions stated as an optimal control problem. The cost functional is a weighted sum of various costs that tries to minimise brain damage and error to the target position. Dhanakoti et al. (2022) also investigate path planning as an optimal control problem with various cost functions, using the model of Rucker (2011). Leibrandt et al. (2017) also consider path planning problems and present software capable of computing a large set of possible tube configurations, as predicted by the kinematic model by Dupont et al. (2009).

Sauerteig et al. (2022) presents an obstacle-avoiding path planning problem for the model derived in Rucker (2011). The authors model sensitive brain areas as ellipsoids that need to be avoided and investigate the solutions found when optimising either one of two cost functions (one minimising arc length and one penalising distance to the target set). The numerical experiments were conducted on "toy data" to demonstrate the idea.

In the current paper we build on the research done in Sauerteig et al. (2022), using the same model, and present a new toolchain that solves path planning in stereotactic neurosurgery. First, building on the work by Hackenberg et al. (2021), we present a new approach to fit ellipsoids to labelled point clouds that identify a target

⋆ This work is funded by the German Research Foundation (DFG, grants FL 989/5-1, OE 253/7-1, SA 773/10-1, WO 2056/11-1).

10.1016/j.ifacol.2023.10.1403

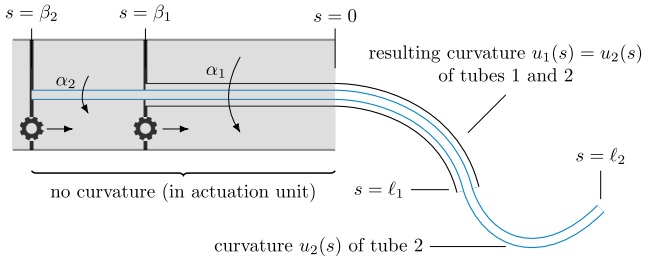

Fig. 1. Two concentric tubes with pre-curvature $\mathbf{u}_i^\star$ extended by β_i and rotated by α_i, $i = 1, 2$ inside the actuation unit. This results in a path $\mathbf{p}(s)$ with curvature $\mathbf{u}(s)$, $s \in [\beta_2, \ell_2]$ denoting arc length. Image taken from Sauerteig et al. (2022).

area, obstacles and the skull. We then present an approach to solve the path planning problem via a homotopy on the obstacle positions, similar to ideas presented in Bergman and Axehill (2018) and De Marinis et al. (2022). We demonstrate the approach with a detailed example using real data labelled by medical professionals. By introducing the homotopy we are able to solve the difficult path planning problem for which the solver could not converge, due to the presence of over a thousand ellipsoidal obstacles.

The outline of the paper is as follows. Section 2 presents the path planning problem. Section 3 describes how the ellipsoids are fit to labelled point clouds and shows the results for a given MRI data set. Section 4 covers the details of the homotopy method we apply to solve the problem, and Section 5 presents some numerics on real data. Finally, Section 6 concludes the paper.

Notation: Given a vector $\mathbf{x} \in \mathbb{R}^n$ and a real symmetric positive definite matrix $Q \in \mathbb{R}^{n\times n}$, $Q \succ 0$, we let $\|\mathbf{x}\|_Q^2 := \mathbf{x}^\top Q \mathbf{x}$. An ellipsoidal set in $\mathbb{R}^3$ with centre $\mathbf{c} \in \mathbb{R}^3$ and matrix $Q \in \mathbb{R}^{3\times 3}$, $Q \succ 0$, is denoted by $\mathrm{Ell}(\mathbf{c}, Q) := \{\mathbf{x} \in \mathbb{R}^3 : \|\mathbf{x} - \mathbf{c}\|_Q^2 \leq 1\}$. The vector $\mathbf{0}_n \in \mathbb{R}^n$ denotes the n-dimensional column vector of zeros. A finite index set is denoted $[1 : K] := \mathbb{Z} \cap [1, K]$, $K \in \mathbb{Z}$. The special orthogonal group on $\mathbb{R}^3$ is denoted by $\mathrm{SO}(3) = \{\mathbf{M} \in \mathbb{R}^{3\times 3} : \mathbf{M}\mathbf{M}^\top = I,\ \det(\mathbf{M}) = +1\}$, and its associated Lie algebra is denoted by $\mathfrak{so}(3) = \{\mathbf{M} \in \mathbb{R}^{3\times 3} : \mathbf{M}^\top = -\mathbf{M}\}$. Given a vector $\mathbf{x} := (x_1, x_2, x_3)^\top \in \mathbb{R}^3$ the wedge operator, $^\wedge : \mathbb{R}^3 \to \mathfrak{so}(3)$, produces a skew-symmetric matrix,

$$\hat{\mathbf{x}} = \begin{pmatrix} 0 & -x_3 & x_2 \\ x_3 & 0 & -x_1 \\ -x_2 & x_1 & 0 \end{pmatrix}.$$

2. THE PATH PLANNING PROBLEM

We consider a concentric tube robot with $n \in \mathbb{N}$ tubes, where the index n refers to the inner-most tube. For $i \in [1 : n]$, each tube has a total length of $L_i \in \mathbb{R}_{\geq 0}$ with a part contained inside the actuation unit, for $s \in [\beta_i, 0]$, $\beta_i \leq 0$, and a part that extends outside the actuation unit, for $s \in [0, \ell_i]$, where s is the arc-length, see Figure 1. Thus, $L_i = \ell_i - \beta_i$. Attached to each tube is a right-handed coordinate frame, continuous with respect to arc-length, with the z-axis tangent to the curve's velocity vector. Each tube's *pre-curvature* (that is, its curvature before interacting with other tubes) as a function of arc-length is specified by $\mathbf{u}_i^\star(s) = (\mathbf{u}_{ixy}^\star(s), u_{iz}^\star(s))^\top \in \mathbb{R}^3$, $\mathbf{u}_{ixy}^\star(s) = (u_{ix}^\star(s), u_{iy}^\star(s))^\top \in \mathbb{R}^2$. Furthermore, each tube's cross-section is an annulus with constant inner and outer diameter, ρ_i^{i} and ρ_i^{o}, respectively; I_i denotes its second moment of area (which is constant) about the x or y axis; E_i denotes its Young's modulus; G_i denotes its shear modulus; and $J_i = 2I_i$ denotes its polar moment. When the tubes are inserted into one another they interact and deform, tracing out a curve with position $\mathbf{p}_i(s)$, rotation $\mathbf{R}_i(s)$ and curvature $\mathbf{u}_i(s) = (\mathbf{u}_{ixy}(s), u_{iz}(s)) = (u_{ix}(s), u_{iy}(s), u_{iz}(s))^\top \in \mathbb{R}^3$. Where the tubes overlap, their positions coincide. However, they are free to rotate about their local z-axes. This rotation is denoted by $\psi_i(s)$. The displacement and rotation of a tube inside the actuation unit, $\beta_i \in \mathbb{R}_{\leq 0}$ and $\alpha_i \in \mathbb{R}$, respectively, produces a tortion on each tube over the section $[\beta_i, 0]$ (inside the actuation unit) resulting in the initial condition, (12). Furthermore, we assume that there is no external load on the tube, resulting in the boundary condition (11). For full details on the derivation of the model refer to Rucker et al. (2010) and Rucker (2011).

We are concerned with the path planning problem (PPP), as stated in Sauerteig et al. (2022):

$$\begin{aligned}
\text{(PPP)} \qquad & \min_{\mathbf{d}\in\mathbb{D}} \quad J(\mathbf{d}) \\
\text{s.t.} \quad & \text{For all } s \in [0, \ell_n] \text{ and all } i \in [1 : n]: \\
& \mathbf{p}_n(s) \in (\mathcal{S} \cap \mathcal{H}) \setminus \mathcal{E}. && (1)\\
& \dot{\mathbf{p}}_n(s) = \mathbf{R}_n(s)\mathbf{e}_3, && (2)\\
& \dot{\mathbf{R}}_n(s) = \mathbf{R}_n(s)\hat{\mathbf{u}}_n(s), && (3)\\
& \dot{\psi}_i(s) = u_{iz}(s), && (4)\\
& \dot{u}_{iz}(s) = A_i \sum_{j\in T(s)} E_j I_j (\mathbf{u}_{ixy}^\star)^\top B_{\psi_{ij}}(s) \mathbf{u}_{jxy}^\star, && (5)\\
& \mathbf{u}_{ixy}(s) = \frac{1}{(EI)(s)} \sum_{j\in T(s)} C_{\psi_{ij}}(s) E_j I_j \mathbf{u}_{jxy}^\star. && (6)\\
& \mathbf{p}_n(0) = \mathbf{p}_n^0 \in \partial\mathcal{S}, && (7)\\
& \mathbf{R}_n(0) = \mathbf{R}_n^0 \in \mathrm{SO}(3), && (8)\\
& \mathbf{p}_n(\ell_n) \in \mathbb{P}_f, && (9)\\
& 0 < L_1 \leq L_2 \leq \cdots \leq L_n. && (10)\\
& u_{iz}(\ell_i) = 0, && (11)\\
& \psi_i(0) = \alpha_i - \beta_i u_{iz}(0), && (12)\\
& \ell_i = L_i + \beta_i, && (13)\\
& 0 \leq \alpha_i < 2\pi, && (14)\\
& -L_i \leq \beta_i \leq 0. && (15)
\end{aligned}$$

The differential equations, (2)-(5), describe the inner-most tube's state as a function of arc-length. Here, $A_i := \frac{E_i I_i}{(EI)(s) G_i J_i}$, $(EI)(s) := \sum_{i\in T(s)} E_i I_i$ and $T(s) := \{i \in [1 : n] : s \leq \ell_i\}$ denotes the tube indices of length at least ℓ_i. Moreover,

$$B_{\psi_{ij}}(s) := \begin{bmatrix} \sin(\psi_i(s) - \psi_j(s)) & -\cos(\psi_i(s) - \psi_j(s)) \\ \cos(\psi_i(s) - \psi_j(s)) & \sin(\psi_i(s) - \psi_j(s)) \end{bmatrix},$$

and

$$C_{\psi_{ij}}(s) := \begin{bmatrix} \cos(\psi_j(s) - \psi_j(s)) & -\sin(\psi_j(s) - \psi_i(s)) \\ \sin(\psi_j(s) - \psi_i(s)) & \cos(\psi_j(s) - \psi_i(s)) \end{bmatrix}.$$

The skull and target are modelled by ellipsoids, $\mathcal{S} = \mathrm{Ell}(\boldsymbol{c}^{\mathcal{S}}, Q^{\mathcal{S}})$ and $\mathbb{P}_f = \mathrm{Ell}(\boldsymbol{c}^{\mathrm{t}}, Q^{\mathrm{t}})$, respectively; $\mathcal{H}$ is a half space containing the brain hemisphere wherein the

target set lies; and $\mathcal{E} \coloneqq \bigcup_{j\in\mathbb{I}^K} \mathcal{E}_j$, with $\mathcal{E}_j = \mathrm{Ell}(\mathbf{c}^{\mathcal{E}_j}, Q^{\mathcal{E}_j})$, $K \in \mathbb{N}$, denotes the ellipsoidal obstacles.

As decision space we consider,

$$\mathbb{D} \coloneqq \{(\mathbf{u}^\star, \mathbf{L}, \boldsymbol{\rho}^{\mathrm{i}}, \boldsymbol{\rho}^{\mathrm{o}}, \boldsymbol{\alpha}, \boldsymbol{\beta}, \mathbf{p}_n^0, \mathbf{R}_n^0) \in \mathbb{R}^{8n+3} \times \mathrm{SO}(3)\}.$$

That is, we choose, for $i = [1:n]$, the precurvatures, $\mathbf{u}_i^\star$ (which we assume constant for all $s \in [\beta_i, \ell_i]$); the tube lengths, L_i; the tube inner and outer diameters, ρ_i^{i} and ρ_i^{o}; the actuator parameters, (α_i, β_i); the initial position of the inner-most tube on the skull, $\mathbf{p}_n^0$; and its initial orientation $\mathbf{R}_n^0$, such that the resulting curve traced out by the inner tube reaches a target area while avoiding a number of obstacles enclosing sensitive brain areas. The tube is also not allowed to cross from one brain hemisphere to the other. The cost function minimises arc length, thus, $J : \mathbb{D} \to \mathbb{R}_{\geq 0}$ is given by,

$$J(\mathbf{d}) \coloneqq \ell_n.$$

If a solution to the problem exists, we denote it by $\bar{\mathbf{d}} \in \mathbb{D}$.

3. OBTAINING THE CONSTRAINTS FROM LABELLED DATA

This section describes how we construct the various constraints appearing in (PPP) from labelled data, which we assume to be point clouds (voxel centres) in $\mathbb{R}^3$ that indicate relevant areas of a patient's brain. These are points that define the skull, $\mathbb{V}^{\mathcal{S}} = \{\boldsymbol{v}_i^{\mathcal{S}}\}_{i\in[1:n_{\mathrm{s}}]}$; the target area, $\mathbb{V}^{\mathrm{t}} = \{\boldsymbol{v}_i^{\mathrm{t}}\}_{i\in[1:n_{\mathrm{t}}]}$; $K \in \mathbb{N}$ obstacles, $\mathbb{V}_j^{\mathrm{o}} = \{\boldsymbol{v}_{ij}^{\mathrm{o}}\}_{i\in[1:n_{\mathrm{oj}}]}$, $j = [1:K]$; and points on a plane that divide the brain into its hemispheres, $\mathbb{V}^{\mathrm{h}} = \{\boldsymbol{v}_i^{\mathrm{h}}\}_{i\in[1:n_{\mathrm{h}}]}$.

Fitting the hyperplane. The plane dividing the hemispheres, which we label $\Pi := \{\mathbf{x} \in \mathbb{R}^3 : \mathbf{x}^\top \boldsymbol{h} = 1\}$, $\boldsymbol{h} \in \mathbb{R}^3$, is found by solving for $\boldsymbol{h}$ in the system of equations,

$$(\boldsymbol{v}_i^{\mathrm{h}})^\top \boldsymbol{h} = 1, \quad i \in [1:n_{\mathrm{h}}],$$

via least-squares linear regression. If all the target points $\mathbb{V}^{\mathrm{t}}$ are contained in one half space defined by this plane, then we take $\mathcal{H}$ to be this half space. Otherwise, if target points appear in both hemispheres, we solve (PPP) twice: once with $\mathcal{H} = \{\mathbf{x} : \mathbf{x}^\top \boldsymbol{h} \leq 0\}$, and once with $\mathcal{H} = \{\mathbf{x} : \mathbf{x}^\top \boldsymbol{h} \geq 0\}$ and choose the best solution of the two problems.

Fitting the skull. The ellipsoid modelling the skull, $\mathcal{S} = \mathrm{Ell}(\boldsymbol{c}^{\mathcal{S}}, Q^{\mathcal{S}})$, is found as a best-fit ellipsoid for all the points in $\mathbb{V}^{\mathcal{S}} \cap \mathcal{H}$ by solving,

$$\begin{aligned} \min_{\boldsymbol{c}^{\mathcal{S}}, Q^{\mathcal{S}}} \quad & \sum_{i\in\mathbb{I}_{\mathrm{new}}^{n_{\mathrm{s}}}} \left(\|\boldsymbol{v}_i^{\mathcal{S}} - \boldsymbol{c}^{\mathcal{S}}\|_{Q^{\mathcal{S}}}^2 - 1\right)^2 \\ \text{s.t.} \quad & Q^{\mathcal{S}} \succ 0, \\ & \boldsymbol{c}^{\mathcal{S}} \in \mathbb{R}^3, \end{aligned}$$

where $\mathbb{I}_{\mathrm{new}}^{n_{\mathrm{s}}} := \{i \in [1:n_{\mathrm{s}}] : \boldsymbol{v}_i^{\mathcal{S}} \in (\mathbb{V}^{\mathcal{S}} \cap \mathcal{H})\}$.

By using fewer points in the fitting we obtain faster execution times without loss of accuracy. We achieve positive definiteness of a matrix Q with rotation matrices, $Q = R^\top M R$, with $M \in \mathbb{R}^{3\times 3}$, a diagonal matrix with positive entries on the main diagonal, and $R \in \mathrm{SO}(3)$, described by quaternions. This formulation allows for setting constraints of the eigenvalues of Q easily.

Fitting the target. The target area is modelled as an ellipsoid enclosed by the target points. Points on its boundary, $\partial\mathbb{V}^{\mathrm{t}}$, may be found with MATLAB's `boundary` -function. Let δ_{MRI} denote the minimal distance between any two points of $\mathbb{V}^{\mathrm{t}}$. If one of the ellipsoid's semi-axes was shorter than δ_{MRI}, it could lie between all the target points and thus exit the point cloud, so the eigenvalues of Q^{t} are constrained to prevent this, resulting in the optimization problem,

$$\begin{aligned} \min_{\boldsymbol{c}^{\mathrm{t}}, Q^{\mathrm{t}}} \quad & \sum_{i\in\mathbb{I}_{\mathrm{new}}^{n_{\mathrm{t}}}} \|\boldsymbol{v}_i^{\mathrm{t}} - \boldsymbol{c}^{\mathrm{t}}\|_{Q^{\mathrm{t}}}^2 \\ \text{s.t.} \quad & \mathrm{eig}(Q^{\mathrm{t}}) > \left(\frac{2}{\delta_{\mathrm{MRI}}}\right)^2 \\ & \|\boldsymbol{v}_i^{\mathrm{t}} - \boldsymbol{c}^{\mathrm{t}}\|_{Q^{\mathrm{t}}}^2 \geq 1 \quad \forall\, i \in \mathbb{I}_{\mathrm{new}}^{n_{\mathrm{t}}}, \end{aligned}$$

where $\mathbb{I}_{\mathrm{new}}^{n_{\mathrm{t}}} := \{i \in [1:n_{\mathrm{t}}] : \boldsymbol{v}_i^{\mathrm{t}} \in \partial\mathbb{V}^{\mathrm{t}}\}$, so that,

$$\mathbb{P}_f = \left\{\boldsymbol{x} : \|\boldsymbol{x} - \boldsymbol{c}^{\mathrm{t}}\|_{Q^{\mathrm{t}}}^2 \leq 1\right\}.$$

The minimisation of the target points' Q^{t}-distance is equivalent to maximising the ellipsoid's volume, the product of the eigenvalues of M, but with faster convergence and more consistent results.

Fitting the obstacles. The same trick from the previous subsection is used in the formulation of enclosing ellipsoids for the obstacles. For an obstacle set $\mathbb{V}_j^{\mathrm{o}}$ we solve,

$$\begin{aligned} \min_{\boldsymbol{c}_j^{\mathrm{o}}, Q_j^{\mathrm{o}}} \quad & -\sum_{i\in\mathbb{I}_{\mathrm{new}}^{n_{\mathrm{oj}}}:} \|\boldsymbol{v}_{ij}^{\mathrm{o}} - \boldsymbol{c}_j^{\mathrm{o}}\|_{Q_j^{\mathrm{o}}}^2 \\ \text{s.t.} \quad & Q_j^{\mathrm{o}} \succ 0 \\ & \|\boldsymbol{v}_{ij}^{\mathrm{o}} - \boldsymbol{c}_j^{\mathrm{o}}\|_{Q_j^{\mathrm{o}}}^2 \leq 1 \quad \forall\, i \in \mathbb{I}_{\mathrm{new}}^{n_{\mathrm{oj}}} \end{aligned} \tag{16}$$

where $\mathbb{I}_{\mathrm{new}}^{n_{\mathrm{oj}}} := \{i \in [1:n_{\mathrm{oj}}] : \boldsymbol{v}_{ij}^{\mathrm{o}} \in \mathbb{V}_j^{\mathrm{o}} \cap \mathcal{H}\}$. This provides the enclosing ellipsoids, $\mathcal{E}_j = \left\{\boldsymbol{x} : \|\boldsymbol{x} - \boldsymbol{c}_j^{\mathrm{o}}\|_{Q_j^{\mathrm{o}}}^2 \geq 1\right\}$.

Division of obstacle points. When fitting an obstacle ellipsoid we want to cover as many obstacle points as possible while minimizing the volume that contains no such points. One major contributor to this problem is if non-connected areas are captured by the same ellipsoid, as might happen with the k-means algorithm, shown by Hackenberg et al. (2021). Applying DBSCAN, a density-based clustering algorithm by Ester et al. (1996), beforehand can alleviate this flaw. The distance δ_{MRI} is used as the search radius for DBSCAN. To evaluate how well the ellipsoids cover the obstacle points and the surrounding area, the coverage is calculated as the number of obstacle points divided by the number of grid points on the MRI grid inside the cluster. Algorithm 1 shows the pseudo-code describing the steps.

Numerical results. Figures 2-4 show the optimisation results for the three different types of ellipsoids. In Fig. 2, only the skull points in the admissible half-space are displayed. It shows that an ellipsoid is a good approximation for the skull. As mentioned, the ellipsoid in Fig. 3 covers a larger volume than the voxels marked as obstacles. The target modelling is successful as well, still the ellipsoid underestimates the size of the target region. Overall, this problem has 1179 obstacle ellipsoids, partly shown in Fig. 6.

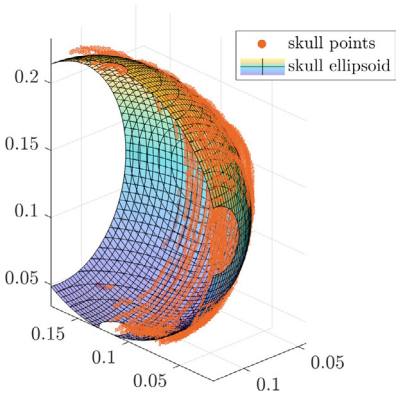

Fig. 2. Best-fit ellipsoid of the skull in allowed hemisphere.

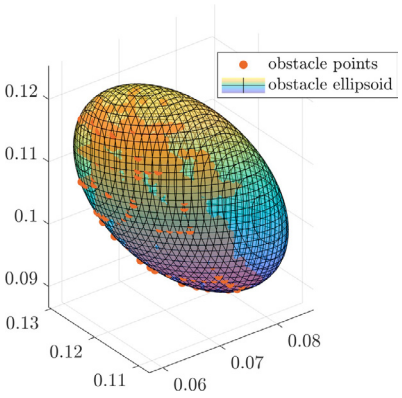

Fig. 3. Enclosing ellipsoid as an approximation for the obstacles.

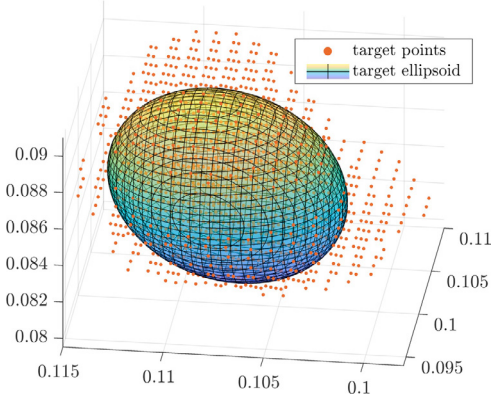

Fig. 4. The target set is modelled as an ellipsoid enclosed by the point cloud.

Algorithm 1 Clustering of obstacle points

Require: obstacle points $\boldsymbol{v}^{\mathrm{o}}$ and threshold c_{th}
Cluster $\boldsymbol{v}^{\mathrm{o}}$ using DBSCAN to get $\boldsymbol{v}^{\mathrm{o}}_i$.
for each i **do**
  while true **do**
    Cluster $\boldsymbol{v}^{\mathrm{o}}_i$ with k-means to get $\boldsymbol{v}^{\mathrm{o}}_{ij}$.
    for each j **do**
      Solve (16) with $\boldsymbol{v}^{\mathrm{o}}_{ij}$.
    end for
    if $\frac{\#\text{ MRI grid points in ellipsoids}}{\#\text{ obstacle points in ellipsoid}} \leq c_{\mathrm{th}}$ **then**
      Increase the number of clusters for k-means.
    else
      Exit the while loop.
    end if
  end while
  Add the j ellipsoids to the obstacle set.
end for

4. SOLUTION APPROACH VIA HOMOTOPY

With realistic data (with hundreds of ellipsoids) numerical solvers often do not converge when applied to (PPP). Thus, using similar ideas from Bergman and Axehill (2018) and De Marinis et al. (2022), we introduce a homotopy on some of the obstacles' positions, where at the one extreme they are removed from the skull's interior, and at the other they are located at their original position. We then iteratively solve relaxed problems, using the solution with a current parameter as the initial guess for the solution with the next parameter (see Algorithm 2).

For a given *homotopy parameter* $\lambda \in [0,1]$ the relaxed problem reads,

$$
\begin{aligned}
(\mathrm{PPP}^{\lambda}) \qquad & \min_{\mathbf{d}\in\mathbb{D}} \quad J(\mathbf{d}) \\
\text{s.t.} \quad & \text{For all } s \in [0,\ell_n] \text{ and all } i \in [1:n]: \\
& \mathbf{p}_n(s) \in (\mathcal{S}\cap\mathcal{H}) \setminus \mathcal{E}^{\mathrm{fix}}, \\
& \mathbf{p}_n(s) \in (\mathcal{S}\cap\mathcal{H}) \setminus \mathcal{E}^{\lambda}, \\
& (2)-(15).
\end{aligned}
$$

Here we let

$$\mathcal{E}^{\mathrm{fix}} = \bigcup_{j\in\mathbb{I}^{\mathrm{fix}}} \mathcal{E}_j,$$

where $\mathbb{I}^{\mathrm{fix}} \subseteq [1:K]$ are the indices of ellipsoids we do *not* perturb; and

$$\mathcal{E}^{\lambda} = \bigcup_{j\in[1:K]\setminus\mathbb{I}^{\mathrm{fix}}} \mathcal{E}^{\lambda}_j,$$

where

$$\mathcal{E}^{\lambda}_j = \mathrm{Ell}([1-\lambda]\mathbf{c}^{\mathrm{init}}_j + \lambda\mathbf{c}^{\mathrm{o}}_j), Q^{\mathrm{o}}_j),$$

are ellipsoids we do. If a solution is found we denote it by $\bar{\mathbf{d}}^{\lambda}$. Thus, λ moves the chosen ellipsoids along the line segment that connects their original positions, $\mathbf{c}^{\mathrm{o}}_j$, with arbitrary user-specified positions, $\mathbf{c}^{\mathrm{init}}_j$, where the entire ellipsoid $\mathcal{E}_j$ is located outside the skull. The *homotopy algorithm* we employ is presented in Algorithm 2.

Algorithm 2 Homotopy Algorithm

Require: initial guess $\mathbf{d}^0$; step size $\Delta > 0$
$\lambda \leftarrow 0$, $\mathbf{d} \leftarrow \mathbf{d}^0$.
while $\lambda < 1$ **do**
  try solve PPP^{λ} with $\mathbf{d}$ as initial guess.
  if solution to PPP^{λ} is found **then**
    $\mathbf{d} \leftarrow \bar{\mathbf{d}}^{\lambda}$, $\lambda \leftarrow \min\{1, \lambda+\Delta\}$
  else
    break while loop
  end if
end while
return $\mathbf{d}$, λ

Heuristic for calculating $\mathbf{c}^{\mathrm{init}}_j$**.** Let $\mathbf{p}^a = \mathbf{p}(0)$ and $\mathbf{p}^b = \mathbf{p}(\ell_n)$ denote the solution with $\lambda = 0$ (i.e., the easily found solution with the obstacles out of the way). All the non-fixed obstacles are shifted orthogonally from the line segment connecting $\mathbf{p}^a$ and $\mathbf{p}^b$. The factor

$$a_i = \frac{(\boldsymbol{c}^{\mathrm{o}}_i - \mathbf{p}^a)^{\top}(\mathbf{p}^b - \mathbf{p}^a)}{\|(\mathbf{p}^b - \mathbf{p}^a)\|_2^2}$$

is needed to find the point closest on the line segment

$$\boldsymbol{l}_i = \begin{cases} \mathbf{p}^a, & \text{if } a_i < 0 \\ \mathbf{p}^a + a_i(\mathbf{p}^b - \mathbf{p}^a), & \text{if } 0 \leq a_i \leq 1 \\ \mathbf{p}^b, & \text{if } a_i > 1 \end{cases}.$$

Thus, the user-specified positions

$$\mathbf{c}^{\mathrm{init}}_i = \boldsymbol{c}^{\mathrm{o}}_i + 0.4\frac{\boldsymbol{c}^{\mathrm{o}}_i - \boldsymbol{l}_i}{\|\boldsymbol{c}^{\mathrm{o}}_i - \boldsymbol{l}_i\|_2}, \ \forall\, i \in ([1:K]\setminus\mathbb{I}^{\mathrm{fix}})$$

are shifted to a distance of 400 mm from the line segment, which is typically outside of the skull. Fig. 5 shows the approach on an example.

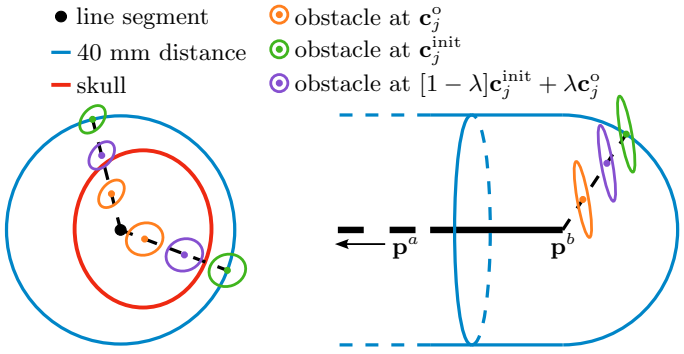

Fig. 5. The obstacle centres are pushed away perpendicular to the line segment connecting the entry and terminal point of the initial guess.

5. NUMERICAL EXAMPLE

We solve a problem with three tubes. We take $u^{\star}_{y,i} = 0$, $L_i = 600\,\text{mm}\ \forall\ i \in [1,3]$, and $\rho_1^{\circ} = 8\,\text{mm}$. We consider tubes made from nitinol (nickel titanium), with Young's modulus $E = 58$ GPa and sheer modulus $G = E/2(1+\nu)$, $\nu = 0.3488$. For the original problem (PPP), with its 1179 obstacles, the solver could not converge. However, a solution was found (where $\lambda = 1$) via the homotopy algorithm, with $\Delta = 0.1$. Table 1 shows the resulting optimal solution for tubes 2 and 3 (it was found that $\ell_1 = 0$).

Table 1. Solution in numerical example

Variable	ℓ_2	ℓ_3	$u^{\star}_{x,2}$	$u^{\star}_{x,3}$
Value	13.2 mm	40.1 mm	$9.99\,\text{m}^{-1}$	$4.55\,\text{m}^{-1}$
Variable	α_2	α_3	β_2	β_3
Value	1.5405	4.7425	−0.587 m	−0.56 m
Variable	ρ_2^{i}	ρ_2°	ρ_3^{i}	ρ_3°
Value	0.004	0.0053	0.0013	0.0026
Variable	$\mathbf{p}_n^0$			
Value	$[0.0967, 0.0769, 0.0536]^{\top}$			
Variable	$\mathbf{q}_n^0$			
Value	$[0.6983, 0.1727, -0.3151, -0.6190]^{\top}$			

The quaternion, $\mathbf{q}_n^0$, specifies the rotation matrix $\mathbf{R}_n^0$. Fig. 6 shows the optimised cannula navigating through the field of the 45 closest obstacles, starting on the skull and entering the target area. Fig. 7 shows the solution without the obstacles.

We use CasADi by Andersson et al. (2019) to formulate the optimisation problem, while (PPP$^{\lambda}$) is solved with IPOPT by Wächter and Biegler (2006). Even though interior-point methods are known to be hard to warm-start (see for example John and Yıldırım (2008)), we show that they work well in this problem. Table 2 presents the parameters used in IPOPT.

Table 2. IPOPT parameters

warm_start_init_point	yes
mu_init	1e-8
warm_start_mult_bound_push	1e-10
warm_start_slack_bound_push	1e-10
warm_start_bound_push	1e-8
warm_start_bound_frac	1e-8
warm_start_slack_bound_frac	1e-10

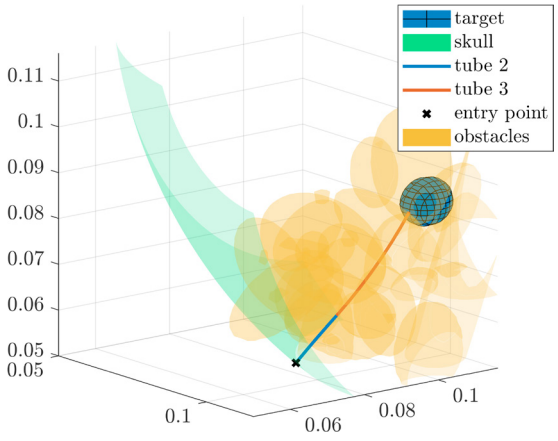

Fig. 6. The solution to the given case-study reaching from the skull to the target position. The 45 ellipsoids closest to the cannula are displayed.

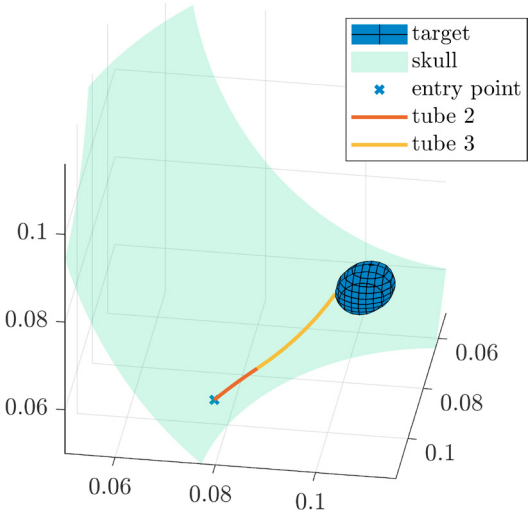

Fig. 7. The solution without the obstacles.

6. CONCLUSION

We tackled a challenging optimal path planning task for a concentric tube continuum robot through a geometrically constrained space and presented a numerical example with data from a real-world example of stereotactic neurosurgery. From labelled MRI or CT scans as a starting point, we formulate easily solvable optimisation problems for condensing the point clouds to a set of ellipsoidal constraints. For the large number of points belonging to the obstacles, we propose an algorithm combining DBSCAN and the k-means-algorithm for separating and clustering the obstacles. By using homotopy methods, we enable the

solution of the path planning problem, for which solvers don't initially converge.

There are many areas on which future research may focus. First, the homotopy algorithm is not guaranteed to converge as λ tends to 1 and conditions on the problem data that imply this should be investigated. Second, in moving the obstacles with the homotopy parameter we did not take care to prevent topological changes in the free space where the tubes may manoeuvre. Though we were able to find a solution to the problem we considered, these topological changes may result in discontinuities of the optimal paths from one iteration of λ to the next, which could cause infeasibility. Third, by using the homotopy approach the final path may in fact only be locally optimal: a result of "slightly" perturbing previously-found solutions.

REFERENCES

Andersson, J.A.E., Gillis, J., Horn, G., Rawlings, J.B., and Diehl, M. (2019). CasADi – A software framework for nonlinear optimization and optimal control. *Mathematical Programming Computation*, 11(1), 1–36.

Bergeles, C., Gosline, A.H., Vasilyev, N.V., Codd, P.J., Pedro, J., and Dupont, P.E. (2015). Concentric tube robot design and optimization based on task and anatomical constraints. *IEEE Transactions on Robotics*, 31(1), 67–84.

Bergman, K. and Axehill, D. (2018). Combining homotopy methods and numerical optimal control to solve motion planning problems. In *2018 IEEE Intelligent Vehicles Symposium (IV)*, 347–354.

Burgner, J., Gilbert, H.B., and Webster, R.J. (2013). On the computational design of concentric tube robots: Incorporating volume-based objectives. In *2013 IEEE International Conference on Robotics and Automation*, 1193–1198.

De Marinis, A., Iavernaro, F., and Mazzia, F. (2022). A minimum-time obstacle-avoidance path planning algorithm for unmanned aerial vehicles. *Numerical Algorithms*, 89(4), 1639–1661.

Dhanakoti, S., Maddocks, J., and Weiser, M. (2022). Navigation of concentric tube continuum robots using optimal control. In *Proceedings of the 19th International Conference on Informatics in Control, Automation and Robotics*, 146–154.

Dupont, P.E., Lock, J., Itkowitz, B., and Butler, E. (2009). Design and control of concentric-tube robots. *IEEE Transactions on Robotics*, 26(2), 209–225.

Ester, M., Kriegel, H.P., Sander, J., Xu, X., et al. (1996). A density-based algorithm for discovering clusters in large spatial databases with noise. In *Proceedings of 2nd International Conference on Knowledge Discovery and Data Mining*, volume 96, 226–231.

Flaßkamp, K., Worthmann, K., Mühlenhoff, J., Greiner-Petter, C., Büskens, C., Oertel, J., Keiner, D., and Sattel, T. (2019). Towards optimal control of concentric tube robots in stereotactic neurosurgery. *Mathematical and Computer Modelling of Dynamical Systems*, 25(6), 560–574.

Gilbert, H.B., Rucker, D.C., and Webster III, R.J. (2016). Concentric tube robots: The state of the art and future directions. *Robotics Research*, 253–269.

Granna, J., Nabavi, A., and Burgner-Kahrs, J. (2019). Computer-assisted planning for a concentric tube robotic system in neurosurgery. *International Journal of Computer Assisted Radiology and Surgery*, 14(2), 335–344.

Greiner-Petter, C. and Sattel, T. (2017). On the influence of pseudoelastic material behaviour in planar shape-memory tubular continuum structures. *Smart Materials and Structures*, 26(12), 125024.

Ha, J., Fagogenis, G., and Dupont, P.E. (2018). Modeling tube clearance and bounding the effect of friction in concentric tube robot kinematics. *IEEE Transactions on Robotics*, 35(2), 353–370.

Hackenberg, A., Worthmann, K., Pätz, T., Keiner, D., Oertel, J., and Flaßkamp, K. (2021). Neurosurgery planning based on automated image recognition and optimal path design. *at-Automatisierungstechnik*, 69(8), 708–721.

John, E. and Yıldırım, E.A. (2008). Implementation of warm-start strategies in interior-point methods for linear programming in fixed dimension. *Computational Optimization and Applications*, 41(2), 151–183.

Leibrandt, K., Bergeles, C., and Yang, G.Z. (2017). Concentric tube robots: Rapid, stable path-planning and guidance for surgical use. *IEEE Robotics & Automation Magazine*, 24(2), 42–53.

Lyons, L.A., Webster, R.J., and Alterovitz, R. (2009). Motion planning for active cannulas. In *IEEE/RSJ International Conference on Intelligent Robots and Systems*, 801–806.

Peikert, S., Kunz, C., Fischer, N., Hlaváč, M., Pala, A., Schneider, M., and Mathis-Ullrich, F. (2022). Automated linear and non-linear path planning for neurosurgical interventions. In *IEEE International Conference on Robotics and Automation*, 7731–7737.

Rucker, D.C., Jones, B.A., and Webster III, R.J. (2010). A geometrically exact model for externally loaded concentric-tube continuum robots. *IEEE Transactions on Robotics*, 26(5), 769–780.

Rucker, D.C. (2011). *The mechanics of continuum robots: model-based sensing and control*. PhD dissertation, Vanderbilt University.

Sauerteig, P., Hoffmann, M.K., Mühlenhoff, J., Miccoli, G., Keiner, D., Urbschat, S., Oertel, J., Sattel, T., Flaßkamp, K., and Worthmann, K. (2022). Optimal path planning for stereotactic neurosurgery based on an elastostatic cannula model. *IFAC-PapersOnLine*, 55(20), 600–605.

Torres, L.G. and Alterovitz, R. (2011). Motion planning for concentric tube robots using mechanics-based models. In *2011 IEEE/RSJ International Conference on Intelligent Robots and Systems*, 5153–5159.

Wächter, A. and Biegler, L.T. (2006). On the implementation of an interior-point filter line-search algorithm for large-scale nonlinear programming. *Mathematical Programming*, 106(1), 25–57.

Webster, R.J., Okamura, A.M., and Cowan, N.J. (2006). Toward active cannulas: Miniature snake-like surgical robots. In *2006 IEEE/RSJ International Conference on Intelligent Robots and Systems*, 2857–2863.

Webster, R.J., Swensen, J.P., Romano, J.M., and Cowan, N.J. (2009). Closed-form differential kinematics for concentric-tube continuum robots with application to visual servoing. In *Experimental Robotics*, 485–494. Springer.